Population Balance Modeling of Aerated Stirred Vessels Based on CFD

Bart C. H. Venneker, Jos J. Derksen, and Harrie E. A. Van den Akker
Kramers Laboratorium voor Fysische Technologie, Delft University of Technology,
2628 BW Delft, The Netherlands

A developed model predicts local gas fraction and bubble-size distributions for turbulent gas dispersion in a stirred vessel, based on the population balance equations (PBE), with relations taken from literature for bubble coalescence and breakup derived from isotropic turbulence theory. The transport of bubbles throughout the vessel is simulated by a scaled single-phase flow field obtained by CFD simulations. Model predictions for the gas fractions in pseudoplastic Xanthan solutions are compared with local measurements and agree well qualitatively. This formulation overcomes the necessity of choosing a constant bubble size throughout the domain, as is done in two-fluid models and is, therefore, more reliable in mass-transfer calculations.

Introduction

Stirred vessels are widely used, among other things, in process industries for (bio)chemical reactions involving more than one phase. Equipped with an impeller revolving at high speed and operated in the turbulent flow regime, stirred vessels are generally considered useful devices for creating a large interfacial contact area between the phases, thereby promoting mass transfer. Nowadays, however, awareness is growing among chemical engineers that, under conditions typical of commercial operation, "intensity" and "quality" of flow, turbulent kinetic energy, turbulent eddies, volume fractions of phases, concentrations of species, and interfacial contact area are never uniformly distributed throughout the vessel. Large values of velocities, kinetic energy, and energy dissipation rate are found in the impeller region, while, near the walls and the top of the vessel, the flow is often more quiescent. As a result, in the case of multiple-phase reactors, the spatial distribution of the phases may be very uneven; the same applies to bubble and droplet sizes in aerated stirred vessels and in agitated liquid-liquid dispersion, respectively. Overall reactor efficiency might increase if, in the more quiescent regions of a stirred vessel, a larger part of the interfacial mass transfer could be effected.

Current methods for designing and improving multiphase reactors, however, are predominantly based on empirical correlations for overall quantities such as power consumption and mixing times. These correlations have several drawbacks: they do not reflect the details of the physics involved in mass transfer and are only applicable in the narrow range of operating conditions for which they were determined. A new design tool can be found in the use of computational fluid dynamics (CFD) techniques. The improvements attained over the last three decades in the areas of turbulence modeling, grid-meshing, and numerical methods now make it possible to perform reliable three-dimensional (3-D) simulations, even for a difficult system as a stirred vessel.

In the case of multiphase flow, the situation is more complex. Transport equations for mass, momentum, and turbulence properties have to be solved for each individual phase. These equations, however, suffer from a lack of universal agreement as to a generally valid formulation of the interfacial transfer terms. In addition, turbulence of multiphase flows is an area hardly covered by fundamental studies as to its dynamics. As the pertinent transport equations are highly coupled and nonlinear, an efficient, yet robust, solution technique for the resulting large sets of algebraic equations is not readily available (Lathouwers and van den Akker, 1996; van Santen et al., 1996).

In general, the continuum phase is treated by an Eulerian approach. For the dispersed phase, two options are available.

Correspondence concerning this article should be addressed to J. J. Derksen.
Current address of B. C. H. Venneker: Laboratory for Materials Science, Delft University of Technology, Delft, The Netherlands.

In case of (very) small loadings, the dispersed phase may be represented by a finite number of particles the motion of which is tracked in a Lagrangian manner. For high loading or if particle-particle interactions are dominant, the Eulerian approach is preferred, based on the two-fluid model (Ishii, 1975). Examples of the latter approach for the simulation of two-phase stirred reactors can be found in Issa and Gosman (1981), Gosman et al. (1992), Morud and Hjertager (1996), Djebbar et al. (1996), and Jenne and Reuss (1997). An alternative method, introduced by Bakker and van den Akker (1994) (see also Bakker, 1992), exploited a slip velocity model and an effective coalescence-redispersion model with a view to deriving a spatial gas fraction distribution from the single-phase flow field obtained via a CFD simulation. A common feature of all these models is the use of a single bubble size. While this may be a reasonable approach for noncoalescing media, in general this may limit the application of all these models.

The objective of the present work is to develop a model which is possible to obtain local bubble-size distributions, and, hence, local gas fractions and mass-transfer rates in an aerated stirred vessel. The model is formulated in terms of population balance equations (PBEs) and has been implemented by Venneker (1999) in the in-house code DAWN. Breakup and coalescence of bubbles is modeled in a fundamental way using isotropic turbulence theory. One of the assumptions made in the model is that gas bubbles do not significantly alter the flow field. Given a prediction of the single-phase flow field, the flow field in gassed conditions can be obtained by a scaling of the single-phase flow field with only the (experimentally determined) drop in power-consumption as a parameter. We will call this 1.5-way coupling. This limits the application of this model to low gas loadings (0–5%), but it offers a more accurate method to predict mass-transfer rates than the present two-fluid models.

General Formulation of the Model

Population balance equations

The key reason why fluid-particle systems may be modeled in terms of population balance equations (PBEs) is the dynamics of the particle-size distribution of interest. The dynamics may only be due to processes by which particles gradually increase and/or decrease in size (such as in response to variations in the chemical composition in the liquid phase), but also due to processes involving continuous interactions between individual particles (such as agglomeration, coalescence, and breakup). Rather than following individual particles, as is done in particle tracking, a continuum approach based on particle statistics is pursued. The concept of PBE, which was first presented by Hulburt and Katz (1964), is now being used in many applications, particularly in the field of crystallization, including the production of margarine. Further references on PBE can be found in the general review of Ramkrishna (1985), as well as in the review of the application of population balances to chemical reactors due to Ritchie and Togby (1978). The combination of PBEs and CFD is relatively new.

In general, the PBE is a balance equation of the number density probability of some particle property. In the present application, the particle property $\boldsymbol{x}$ is the number density probability of particles with bubble size d, but one can also think of the particle age as a modeled property in order to determine the residence time distribution.

The PBE in its most general form is given by Ramkrishna (1985) as

$$\frac{\partial n(\boldsymbol{x}, \boldsymbol{r}, t)}{\partial t} + \nabla_{\boldsymbol{x}} \cdot \dot{\boldsymbol{x}} n(\boldsymbol{x}, \boldsymbol{r}, t) + \nabla_{\boldsymbol{r}} \cdot \boldsymbol{v}_p n(\boldsymbol{x}, \boldsymbol{r}, t) = B(\boldsymbol{x}, \boldsymbol{r}, \boldsymbol{Y}, t) - D(\boldsymbol{x}, \boldsymbol{r}, \boldsymbol{Y}, t) \quad (1)$$

in which $n(\boldsymbol{x}, \boldsymbol{r}, t)$ is the number density probability of the property under consideration as function of the property vector $\boldsymbol{x}$, the physical position of the particle $\boldsymbol{r}$ and time t. $\dot{\boldsymbol{x}}$ is the growth rate of the particle due to processes other than interaction with other particles, and $\boldsymbol{v}_p$ is the velocity of the particle. The continuous phase variables which may affect the particle property, are represented by the vector $\boldsymbol{Y}(\boldsymbol{r}, t)$.

On the righthand side of Eq. 1, $B(\boldsymbol{x}, \boldsymbol{r}, \boldsymbol{Y}, t)$ represents the rate of production (**birth**) and $D(\boldsymbol{x}, \boldsymbol{r}, \boldsymbol{Y}, t)$ the rate of destruction (**death**) of particles of a particular state $(\boldsymbol{x}, \boldsymbol{r})$ at time t. In the case of bubble size as the particle property, bubbles of a certain diameter d are continuously formed by either breakage of larger bubbles or coalescence of smaller bubbles. Similarly, bubbles of diameter d are continuously destroyed by breakage into smaller bubbles, and by coalescence into larger ones. The functions that describe these breakup and coalescence processes have to be specified further. Their specific form may vary for different particle-fluid systems and for the particle property under consideration.

Gas-Dispersion Modeling. In the case of gas-dispersion modeling where the bubble diameter is the most important bubble property, the following forms have been adopted for the birth and death functions (Tsouris and Tavlarides, 1994)

$$B(d, t) = \frac{1}{2}\int_0^d p(d'', d')h(d'', d')n(d'', t)n(d', t)\mathrm{d}d' + \int_d^\infty \eta(d, d')\nu(d')g(d')n(d', t)\mathrm{d}d' \quad (2)$$

in which $d'' = (d^3 - d'^3)^{1/3}$, and

$$D(d, t) = n(d, t)\int_0^\infty p(d, d')h(d, d')n(d', t)\mathrm{d}d' + g(d)n(d, t) \quad (3)$$

Note that the dependency on $\boldsymbol{r}$ and $\boldsymbol{Y}$ has been dropped for brevity only. The various parameters in Eqs. 2 and 3 relate to the following physical mechanisms:

$h(d, d')$: effective swept volume rate of bubbles of diameter d colliding with bubbles of diameter d' [m^3/s]

$p(d, d')$: coalescence efficiency after collision between bubbles of diameter d and d' [—]

$g(d)$: breakage frequency of bubbles of diameter d [$1/s$]

$\eta(d, d')$: daughter probability distribution [$1/m$]

$\nu(d')$: number of bubbles formed from the breakage of a bubble diameter d' [—]

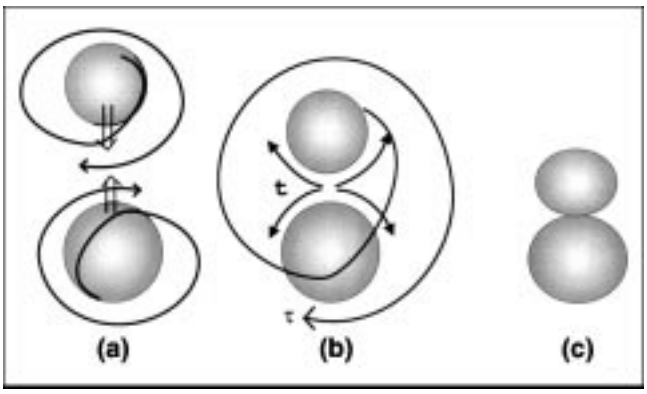

Figure 1. Three steps of coalescence: (a) approach of bubbles; (b) thinning of liquid film; (c) film rupture.

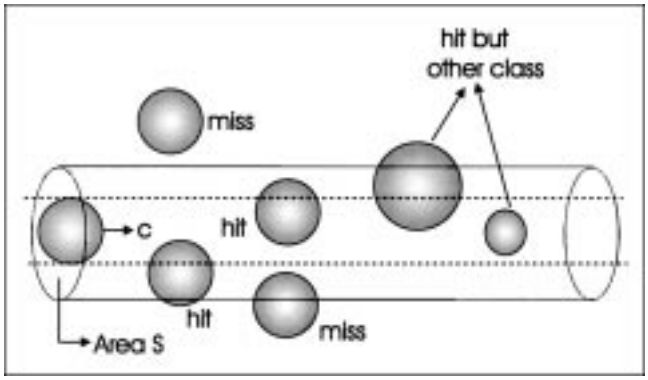

Figure 2. Collision tube of a bubble moving with a relative speed c.

Equations 2 and 3 are general mathematical formulations of the coalescence and breakup processes. The integrals express that bubbles of diameter d can break up into bubbles of any size d' as long as $d' < d$, and that they can coalesce with any other bubble of diameter d'. As a result, the bubble-size distribution is a continuous function. In most cases, analytical solutions of Eq. 1 do not exist, and it has to be solved numerically. In the remainder of this section, the different processes are treated in more detail and the effects of the physical properties of the fluid and the flow on the various functions are discussed.

Coalescence

The process by which two (or more) bubbles coalesce, essentially consists of three successive steps that are drawn in Figure 1. First, bubbles have to collide, trapping a small amount of liquid between them. The second step involves the drainage of liquid out of the film between the adjacent bubble surfaces, while the third and final step is the rupture of the film leading to coalescence. We assume that collisions of bubbles occur due to turbulent transport only. Alternatively, one may include other collision mechanisms such as buoyancy-driven, that is, collisions due to the difference in rise velocities of bubbles of different size, and collisions due to laminar shear (Prince and Blanch, 1990). In the present model, rather than the actual collision frequency, the volume swept by a moving bubble is calculated, from which the number of other bubbles that are hit by this moving bubble can be indirectly determined.

Effective Swept Volume Rate h(d, d'). The volume rate which is swept by a bubble of diameter d is modeled on the analogy of kinetic gas theory. Consider a bubble in an eddy, moving with a relative speed c with respect to other bubbles. In a time Δt, the bubble sweeps a "collision tube" with cross-sectional area $\pi(d + d')^2/4$, in which d' is the diameter of the other bubbles (Figure 2). The effective swept volume rate is then given by

$$h(d, d') = \frac{\pi}{4}(d + d')^2 c \tag{4}$$

An estimate for the relative speed c can be given using the classical theory on isotropic turbulence due to Kolmogorov (1941). It states that, if the distance l between two points in the flow field is much smaller than the turbulence macroscale L, but much larger than the Kolmogorov microscale l_d, the relative velocity is only a function of the energy dissipation rate ϵ and the magnitude of the length l

$$c^2 = v^2(l) = C(\epsilon l)^{2/3} \tag{5}$$

According to one of Kolmogorov's assumptions, eddies much larger than l may contribute little to $v^2(l)$. Two bubbles in such a large eddy may be advected together without approaching each other. An analysis of grid turbulence due to Batchelor (1951) and measurements in stirred vessels and pipes of colliding drops by Kuboi et al. (1972) suggest that the constant C equals 2.0. Using further the radii of the colliding bubbles as a measure for l, we have

$$v^2 = 2.0\epsilon^{2/3}(r + r')^{2/3} = 1.26\epsilon^{2/3}(d + d')^{2/3} \tag{6}$$

Hence, the effective swept volume rate in terms of bubble diameters is given by

$$\boxed{h(d, d') = \frac{\pi}{4}\sqrt{1.26}\,\epsilon^{1/3}(d + d')^{7/3}} \tag{7}$$

Coalescence Efficiency p(d, d'). The second step in bubble coalescence is the drainage of the liquid from between the bubbles until the liquid film, separating the bubbles, reaches a critical thickness. At this point, film rupture occurs, resulting in coalescence. The bubbles have to be in contact for a certain period of time, sufficient for the liquid film to reach the critical thickness. If the bubbles are separated by an incoming eddy before this thickness is reached, no coalescence occurs. On the one hand, turbulence promotes collisions of bubbles, while on the other hand, it decreases the coalescence efficiency. As a measure for the collision efficiency $p(d, d')$, usually the ratio between the average drainage time $\bar{t}$ and the average contact time $\bar{\tau}$ is taken (Prince and Blanch,

1990)

$$p(d, d') = \exp\left[-\frac{\bar{t}}{\bar{\tau}} \right] \tag{8}$$

Figure 1b shows the drainage of the liquid film between two bubbles, which are trapped in an eddy with lifetime τ.

Depending on the viscosities of the two phases and the presence of surfactants, the drainage of the liquid film between two bubbles is modeled in different ways. A useful, more precise conceptual picture is that, when two bubbles approach one another, the interfaces flatten and give rise to a circular disc-like film of liquid in between. The liquid has to drain from this disc when the flat interfaces get closer. For an aqueous-air system, the bubble interfaces are deformable and fully mobile. Film drainage is controlled by inertia and surface tension forces if (Chesters, 1975)

$$\frac{4\mu}{\rho V r} \ll 1 \tag{9}$$

in which V is the approach velocity of the two bubbles.

A relation for the film thickness h can then be derived by solving Bernoulli's equation for the disc (Kirkpatrick and Lockett, 1974)

$$h = h_0 \exp\left[-4t\sqrt{\frac{\sigma}{\rho_c a^2 R_{eq}}} \right] \tag{10}$$

in which R_{eq} is the equivalent bubble radius, given by

$$R_{eq} = \frac{2}{1/r + 1/r'} \tag{11}$$

for the coalescence between two unequally sized bubbles with radii r and r'. To calculate the drainage time, we need estimates for the initial film thickness h_0, for the radius of the thinning disc a, and for the critical thickness h_c at which the film ruptures.

Chesters (1975) gives an estimate for h_0, assuming that the pressure generated between approaching spherical bubbles becomes sufficiently high to cause substantial deformation

$$h_0 = \frac{\rho_c V^2 R_{eq}^2}{4\sigma} \tag{12}$$

Alternatively, a single value may be used for h_0 irrespective of bubble radius. For example, Kirkpatrick and Lockett (1974) used $h_0 = 0.1$ mm in all cases, which is considerably smaller than predicted by Eq. 12.

The radius a actually is a function of time, which complicates the drainage equations substantially. Most authors, therefore, assume that deformation of the bubble surface occurs instantaneously and poses a relation for a. We used a relation due to Chesters (1991)

$$a = R_{eq}\left(\frac{We}{2} \right)^{1/2} = R_{eq}\left(\frac{\rho_c V^2 R_{eq}}{2\sigma} \right)^{1/4} \tag{13}$$

This relation is based on the relative increase in surface area, and, hence, on the surface free energy. The approach velocity V may be set equal to v given by Eq. 6.

Finally, for the critical film thickness h_c, an approach due to Chesters (1991) is adopted that leads to the expression

$$h_c = \left(\frac{A R_{eq}}{8\pi\sigma} \right)^{1/3} \tag{14}$$

with A the Hamaker constant.

The drainage time in the case of deformable, fully mobile interfaces is then given by

$$\boxed{t_{mob} = \frac{1}{4\sqrt{\dfrac{\sigma}{\rho_c a^2 R_{eq}}}} \ln\left(\frac{h_0}{h_c} \right)} \tag{15}$$

The average contact time $\bar{\tau}$ is given by Levich (1962) as

$$\bar{\tau} = \frac{(d + d')^{2/3}}{\epsilon^{1/3}} \tag{16}$$

So, the coalescence efficiency is obtained by substituting Eq. 15 and 16 into 8.

Breakup

Breakup of bubbles in a turbulent flow is caused by turbulent eddies bombing the bubble surface. If the energy of the incoming eddy is sufficiently high to overcome the surface energy, deformation of the surface is the result, which can finally lead to the formation of two or more daughter bubbles. For bubble breakup to occur, the sizes of the bombarding eddies have to be smaller than or equal to the bubble size, since larger eddies only transport the bubble.

In order to model the breakup process, the following simplifications are generally made (Luo and Svendsen, 1996):

(1) The turbulence is isotropic.

(2) Only binary breakage of a bubble is considered ($\nu = 2$).

(3) The breakage volume ratio is a stochastic variable.

(4) The occurrence of breakup is determined by the energy level of the arriving eddy.

(5) Only eddies of a size smaller than or equal to the bubble diameter can cause bubble breakup.

The second and third simplification are supported by experimental observations on bubble breakage by Hesketh et al. (1991).

Breakage Frequency g(d). As stated above, for a bubble to break up, the colliding eddies must have (1) sufficient energy to overcome the increase in surface energy, and (2) a size of the order of the bubble diameter. As a result, breakage fre-

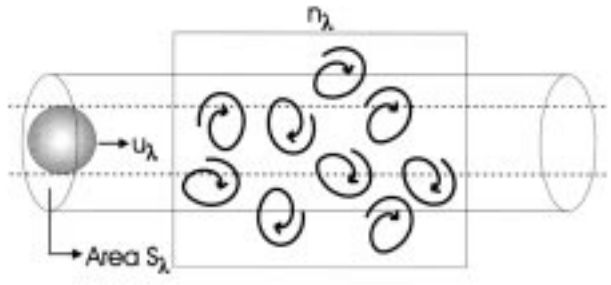

Figure 3. Collision frequency between bubble and eddies.

quency may be thought of as the product of an eddy-bubble collision rate and a breakage efficiency, which both depend on eddy size (Luo and Svendsen, 1996)

$$g(d) = \int_{\lambda_{\min}}^{d} \omega(d, \lambda) p_b(d, \lambda) \mathrm{d}\lambda \tag{17}$$

The eddy-bubble collision rate is modeled in the same way as bubble-bubble collisions

$$\dot{\omega}(d, \lambda) = h(d, \lambda) n_\lambda \tag{18}$$

in which n_λ is the number density probability of eddies with size λ, and $h(d, \lambda)$ is again the swept volume rate now calculated using both a bubble diameter and an eddy size (see Figure 3)

$$h(d, \lambda) = \frac{\pi}{4}(d + \lambda)^2 u_\lambda \tag{19}$$

in which the relative velocity between an eddy and a bubble u_λ may be estimated, on the basis of turbulence theory (Luo and Svendsen, 1996)

$$\overline{u_\lambda^2} = \frac{1.70}{(2\pi)^{2/3}} \epsilon^{2/3} \lambda^{2/3} \tag{20}$$

The number density probability of the eddies n_λ may be estimated with the help of the turbulent energy spectrum $E(k)$, that is, from

$$n_\lambda \frac{1}{2} \frac{\pi}{6} \lambda^3 \overline{u_\lambda^2} \mathrm{d}\lambda = E(k)(1 - \alpha)\mathrm{d}k \tag{21}$$

in which the gas holdup α is used to take into account that only a fraction $(1 - \alpha)$ of the swept volume is occupied by liquid. Substituting Eq. 20 and using, from Hinze (1975), an expression for $E(k)$ yields

$$n_\lambda = \frac{12(1 - \alpha)}{\pi \lambda^4} \tag{22}$$

The final equation for the collision rate is obtained by substituting Eqs. 19, 20, and 22 into Eq. 18

$$\boxed{\omega(d, \lambda) = \frac{\pi}{4}(d + \lambda)^2 \frac{\sqrt{1.70}}{(2\pi)^{1/3}} (\epsilon\lambda)^{1/3} \frac{12(1 - \alpha)}{\pi \lambda^4}} \tag{23}$$

Breakage Efficiency $p_b(d, \lambda)$. When a bubble is hit by an eddy, the probability of breakage not only depends on the energy of the incoming eddy, but also on the cohesive forces which act on the bubble surface. The ratio of disruptive and cohesive forces is expressed by the Weber number

$$We = \frac{\rho_c u^2 d_b}{\sigma} \tag{24}$$

A critical Weber number can be assigned to the situation where cohesive and disruptive forces balance, resulting in a maximum stable bubble size. According to Prince and Blanch (1990), the critical Weber number is 2.3 for air bubbles in water. Here it is assumed that this value also holds for pseudoplastic fluids. As a result, the critical eddy velocity to break a bubble of size d_b is

$$u_c = 1.52 \left(\frac{\sigma}{d_b \rho_c} \right)^{1/2} \tag{25}$$

An exponential relation between u_c^2 and $\overline{u_\lambda^2}$ is assumed for the breakage efficiency, just as for the coalescence efficiency; $p_b(d, \lambda)$ then becomes

$$\boxed{p_b(d, \lambda) = \exp\left(- \frac{u_c^2}{\overline{u_\lambda^2}} \right) = \exp\left(- \frac{(2\pi)^{2/3} 2.3\sigma}{1.70 \epsilon^{2/3} \lambda^{2/3} d_b} \right)} \tag{26}$$

In order to determine the breakage frequency, a lower limit for the eddy size must be set in Eq. 17. Since the $-5/3$ law was used for the eddy velocities, the lower limit is set at the end of the inertial subrange. In terms of wave numbers this equals 0.55 k_d, with k_d as the Kolmogorov wave number (Tennekes and Lumley, 1972). The minimum eddy size then is 11.4 l_d.

Daughter Bubble Distribution $\eta(d, d')$. For calculating the sizes of the daughter bubbles after breakage, it is assumed

that the energy required for the creation of new surface area is the key parameter. It is also assumed that a minimum bubble size exists for the daughter bubbles; otherwise, the probability at the extremes of the distribution would be infinity. Let $e_{\min}$ be the kinetic energy needed to create the smallest and largest bubbles, and $e_{\max}$ be the energy needed to create two equally sized bubbles; then, the daughter bubble probability density function for the breakage of a bubble of size d' is written as (Tsouris and Tavlarides, 1994)

$$\eta(d, d') = \frac{e_{\min} + e_{\max} - e(d)}{\int_0^{\infty} [e_{\min} + e_{\max} - e(d)] \mathrm{d}d} \tag{27}$$

Discretization of the PBEs

In practical situations, one is generally not interested in the number density probability n, but rather in the number density N_i—the number of bubbles of a particular class per unit volume—itself. This number density is defined as

$$N_i(t) = \int_{d_i}^{d_{i+1}} n(d, t) \mathrm{d}d \tag{28}$$

in which $n(d, t)$ follows from Eqs. 2 and 3, convective and dispersive terms being ignored—for the time being—for the sake of simplicity.

The result of the integration is a balance equation for the number densities N_i, in terms of the (unknown) number density probability $n(d, t)$ and is, hence, still unsolvable. To overcome this problem, the bubbles are assumed to be concentrated at a representative size x_i although N_i is the total number of bubbles with sizes between d_i and d_{i+1}. With this assumption, the discretized number density probability can be expressed in terms of the number density

$$n(d, t) = \sum_{i=1}^{M} N_i(t) \delta(d - x_i) \tag{29}$$

with M the total number of bubble classes. Substituting Eq. 29 into Eq. 1 with neglection of the convection and diffusion terms finally gives the general form of the discretized population balance equation

$$\begin{aligned} \frac{\mathrm{d}N_i(t)}{\mathrm{d}t} = \frac{1}{2} & \sum_{\substack{j,k \\ v_i \le (v_j + v_k) \le v_{i+1}}} p(x_j, x_k) h(x_j, x_k) N_j(t) N_k(t) \\ & + \sum_{k > i} N_k(t) \eta(x_i, x_k) \nu(x_i) g(x_k) \\ & - N_i(t) \sum_{k=1}^{M-1} p(x_i, x_k) h(x_i, x_k) N_k(t) \\ & - N_i(t) g(x_i) \end{aligned} \tag{30}$$

Generally, the population balance Eq. 30 (with additional input and output terms) are solved for the agitated vessel (or any other process equipment) as a whole. See the work of Tavlarides and coworkers (Coulaloglou and Tavlarides, 1977; Lewalle et al., 1987; Tsouris and Tavlarides, 1994) on liquid-liquid dispersions in stirred tanks, and that of Prince and Blanch (1990) for bubble columns. The underlying assumption in doing this is that conditions are homogeneous. The average dissipation rate—which is used in the specific functions for the breakage and coalescence—is calculated from the power input.

From real life and from single-phase flow simulations, we know that conditions in a stirred vessel vary greatly from one point to another. In the impeller domain, the conditions in the turbulent regime are mainly such that breakup is dominating, whereas in the more quiescent regions in the upper part of the vessel, coalescence is dominating. The number density of bubbles, their size distribution, and, hence, holdup, is therefore also likely to vary throughout the vessel. Therefore, a more realistic view of multiphase systems can be obtained by solving the M balance equations for each computational grid point. This further has the advantage that bubble velocities, which affect the local values of the number densities, can be taken into account as well. A more systematic approach is then available to study the differences between aqueous systems and more viscous of even non-Newtonian systems.

Bubble Sizes. In order to cover a broad range in bubble volume, the bubble classes are chosen in such a way that the bubble volume in class i is twice that in class $i-1$. Furthermore, it is assumed that only two bubbles are involved in the coalescence process, and that bubbles break up into two bubbles only. The smallest bubbles do not break up and the largest bubbles are not involved in the coalescence process.

The formation of a bubble of size d in size range (x_i, x_{i+1}) due to breakup or coalescence is represented by assigning fractions $f_1(d, x_i)$ and $f_2(d, x_{i+1})$ to bubble populations at x_i and x_{i+1}, respectively. This is necessary because not all coalescence and breakages result in a bubble which has a legitimate size. Consider, for example, three classes of bubbles with volumes $1v$, $2v$, and $4v$. The coalescence of a bubble with volume $1v$ with a bubble of size $2v$ will result in a bubble with a volume of $3v$. Clearly, we have to distribute this new bubble in fractions f_1 and f_2 over the two neighboring classes, in this case $2v$ and $4v$. To determine these two fractions, we need two equations. Of course, the first equation relates to the total volume of the two bubbles, to ensure mass conservation. The second conservation equation is taken here as the conservation of bubble surface $a_b(d)$, since the total bubble surface is important for mass transfer. Alternatively, one may choose to use conservation of the number of bubbles involved in the breakage and coalescence process

$$\begin{aligned} f_1(d, x_i) \cdot v_{b,i} + f_2(d, x_{i+1}) \cdot v_{b,i+1} &= v_b(d) \\ f_1(d, x_i) \cdot a_{b,i} + f_2(d, x_{i+1}) \cdot a_{b,i+1} &= a_b(d) \end{aligned} \tag{31}$$

Both fractions f_1 and f_2 need to be considered in the birth and death processes in Eq. 30. The discretized version of the population balance equation, without convective and disper-

sive terms, is then written as

$$\frac{dN_i(t)}{dt} = \frac{1}{2} \sum_{\substack{j,k \\ v_{b,i} \le (v_{b,j}+v_{b,k}) \le v_{b,i+1}}} f_1(d, x_i)p(x_j, x_k)h(x_j, x_k) \times N_j(t)N_k(t) + \frac{1}{2} \sum_{\substack{j,k \\ v_{b,i-1} \le (v_{b,j}+v_{b,k}) \le v_{b,i}}} f_2(d, x_i)p(x_j, x_k) \times h(x_j, x_k)N_j(t)N_k(t) + \sum_{\substack{j,k \\ v_{b,i} \le (v_{b,k}-v_{b,j}) \le v_{b,i+1}}} f_1(d, x_i) \times \eta(x_i, x_k)\nu(x_k)g(x_k)N_k(t) + \sum_{k=1}^{i-1} f_2(d, x_i)\eta(x_i, x_k)\nu(x_k)g(x_k)N_k(t) - N_i(t)\sum_{k=1}^{M-1} p(x_i, x_k)h(x_i, x_k)N_k(t) - N_i(t)g(x_i) \quad (32)$$

Bubble velocity and shape

In the gas dispersion code DAWN, bubble velocities are calculated as the sum of the liquid velocity and the slip velocity between the two phases

$$\boldsymbol{U}_g = \boldsymbol{U}_{l,g} + \boldsymbol{U}_s \quad (33)$$

in which $\boldsymbol{U}_{l,g}$ denotes the liquid velocity under gassed conditions. The slip velocity $\boldsymbol{U}_s$ can be calculated from a force balance on a bubble

$$\Delta\rho g v_b \hat{\boldsymbol{z}} - \rho_c v_b \frac{W_{l,g}^2}{r}\hat{\boldsymbol{r}} = C_D \frac{1}{2}\rho_c |\boldsymbol{U}_s|\boldsymbol{U}_s \frac{\pi}{4}d^2 \quad (34)$$

in which v_b denotes the bubble volume, $\hat{\boldsymbol{r}}$ is the unit vector in the radial direction, $\hat{\boldsymbol{z}}$ is the unit vector in the axial direction, and $W_{l,g}$ is the tangential component of $\boldsymbol{U}_{l,g}$. The force in the radial direction is the centrifugal force on the bubbles and is optional in the code. The force in the vertical direction is the buoyancy force.

The drag coefficient C_D is a function of the Reynolds number. With only bubble diameters initially given, both C_D and *Re* are unknown. In the case of *Newtonian* fluids, two methods are available to obtain values for the drag coefficient and Reynolds number: an iterative method with a given relationship between C_D and *Re*, or using a unique relation between d and U_s with the bubble diameter as independent variable, from which C_D and *Re* can be calculated. The second method is preferred, because it makes iterations redundant. Several correlations can be used for various two-phase systems (Wallis, 1974; Grace et al., 1976); the experimental data at the basis of these correlations, however, relate to Newtonian fluids only. As similar correlations for *non-Newtonian* fluids are not available, the first method has to be used.

In the literature, limited experimental data is available for the terminal rise (or fall) velocity to drops and bubbles in pseudoplastic fluids. For pseudoplastic liquids, the Reynolds number comprises the flow index

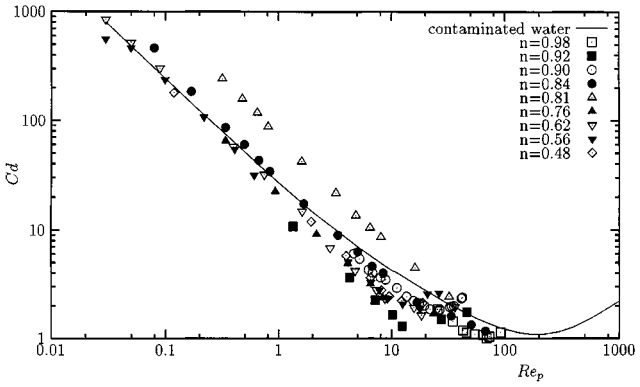

Figure 4. Experimental data for drag coefficient C_D of bubbles in pseudoplastic fluids.

Experimental data due to: Barnett et al. (1966), Haque et al. (1988), and Tsukada et al. (1990).

$$Re_p = \frac{\rho_c u_s^{2-n} d^n}{K} \quad (35)$$

The $C_D - Re_p$ data are plotted in Figure 4. All data (except $n = 0.81 : \Delta$) lay quite close to the experimental drag curve of bubbles in contaminated water, although no data is available for Reynolds numbers higher than 100.

In DAWN, the following iterative procedure is used to calculate the drag coefficient. First, C_D is calculated using approximate correlations for the experimental drag curve of bubbles in contaminated water and an initial estimate of the slip velocity. Secondly, the new slip velocity is calculated, using the obtained value of C_D with

$$u_s = \sqrt{\frac{4\Delta\rho g d}{3\rho C_D}} \quad (36)$$

The iteration is repeated until the difference between the guessed and calculated velocity is smaller than 1%. This slip velocity is then compared with the velocity calculated by the wave theory of Mendelson (1967)

$$u_s = \sqrt{\frac{2.14\sigma}{\rho d} + 0.505 g d} \quad (37)$$

The constants in Eq. 37 have been proposed by Clift et al. (1978). The actual slip velocity used in DAWN is the smallest of the two. It turned out to be necessary to also use the relationship of Mendelson, because the largest bubbles in the simulations could otherwise have slip velocities as high as 40 cm/s. Equation 37 was also used by Tsukada et al. (1990) for the upper limit of slip velocities.

One of the options in DAWN is to correct the bubble velocity for the local void fraction α. This is done according to

Richardson and Zaki (1954)

$$\frac{u_s}{u_\infty} = (1-\alpha)^{q-1} \tag{38}$$

in which q is a function of the Reynolds number Re_p.

Bubble Shapes. Important for the mass transfer—and indirectly for C_D—is an accurate description of the surface area of a bubble. At low Reynolds and Eötvös numbers, interfacial tension and viscous forces are much more important than inertia forces, and the bubble has a spherical shape. At higher Reynolds and Eötvös numbers, the bubbles are more ellipsoidal with varying width (a) over height (b) ratio. The Eötvös number is defined as

$$Eo = \frac{g\rho d_e^2}{\sigma} \tag{39}$$

in which d_e is the diameter of a volume-equivalent sphere. The transition spherical/ellipsoidal (see Figure 2.5 in Clift et al. (1978)) is approximated by

$$\log Re = 1.205 \cdot \exp\left[-1.631 \log Eo\right] \tag{40}$$

The width to height ratio a/b of an ellipse is calculated from a plot presented by Harmathy (1960). No special treatment was introduced for spherical cap bubbles that will occur if $Eo > 40$.

Mass transfer

The mass-transfer coefficient k_l is calculated on the basis of the surface renewal concept of Kawase et al. (1987). This concept is based on Higbie's penetration theory (Higbie, 1935) and the surface renewal model of Danckwerts (1951). In the model, turbulence brings elements of bulk fluid up to the free surface of a bubble, where unsteady mass transfer occurs for a time t_e, after which the element returns to the bulk and is replaced by another. k_l is then given by (Higbie, 1935)

$$k_l = \frac{2}{\sqrt{\pi}}\sqrt{\frac{\mathfrak{D}}{t_e}} \tag{41}$$

The exposure time t_e is further modeled according to the periodic transitional sublayer model of Pinczewski and Sideman (1974). For power-law fluids, t_e is written as (Kawase and Ulbrecht, 1983)

$$t_e = T^{+2}\frac{(K/\rho)^{1/n}}{\nu_0^{2/n}} \tag{42}$$

in which T^+ is a dimensionless bursting time period, and ν_0 is a friction velocity, given by Metkin and Sokolov (1982) as

$$\nu_0 = 2\epsilon^{n/2(1+n)}\left(\frac{K}{\rho}\right)^{1/2(1+n)} \tag{43}$$

Substitution of Eqs. 42 and 43 into Eq. 41 yields

$$k_l = \frac{4}{\sqrt{\pi}}2^{1/n}\frac{1}{T^+}\mathfrak{D}^{1/2}\left(\frac{K}{\rho}\right)^{-1/2(1+n)}\epsilon^{1/2(1+n)} \tag{44}$$

where the factor 4 is included to account for the reduced exposure time at a free surface compared to a rigid surface, and the value of T^+ is taken as 15.0 (Kawase and Ulbrecht, 1983). For Newtonian fluids, Eq. 44 reduces to

$$k_l = 3.01 Sc^{-1/2}(\epsilon\nu)^{1/4} \tag{45}$$

which was also used by Bakker and van den Akker (1994) in their gas dispersion model GHOST!.

The local volumetric mass-transfer coefficient $k_l a$ is calculated when the surface area a_b of each bubble in a grid cell is known. In the case of ellipsoidal bubbles, the surface area is given by

$$a_b = 2\pi a^2\left[1 + \frac{b}{a}\frac{\ln\left(a/b + \sqrt{a^2/b^2 - 1}\right)}{\sqrt{a^2/b^2 - 1}}\right] \tag{46}$$

The summation of all the bubbles in each class then gives the local $k_l a$

$$k_l a = k_l \sum_{i=1}^{M} N_i a_{b,i} \tag{47}$$

Integration of the local values of $k_l a$ over the entire vessel gives the overall mass-transfer coefficient. In the output of DAWN, both the overall value of $k_l a$ and the local values are reported. This makes it possible to identify the regions where the highest mass-transfer rates occur.

Experimental Setup

Global and local measurements of the gas fraction in a stirred vessel have been performed to validate the predictions by the PBE model. The diameter T of the baffled vessel was 0.441 m, a six-blade Rushton type impeller was used with diameter $D = 0.147$ m (Figure 5). The working fluid was a 0.075 wt. % solution of Xanthan gum (trade name Keltrol). Its rheological behavior could well be described with the following power-law parameters: $K = 0.0367$ kg s^{2-n}/m and $n = 0.65$. The solution had a surface tension of $\sigma = 0.0672$ *N/m*.

A ring sparger was placed midway between the flat vessel bottom and the impeller disc. The diameter of the sparger was the same as the impeller disc diameter. In all cases, air was used as the disperse phase. In the experiments, a gas-flow rate of $Q_g = 0.85$ L/s was used. The impeller speed was $N = 5.0$ rev/s, giving a power input of $P_g = 0.29$ W/kg. With these experimental conditions, the gas was completely dispersed.

The power drawn was calculated from measuring the rotational speed of the impeller and the torque exerted by the impeller. The overall gas holdup was visually determined by reading the liquid level. Local measurements of the gas fraction were determined with an optical fiber probe (Venneker, 1999).

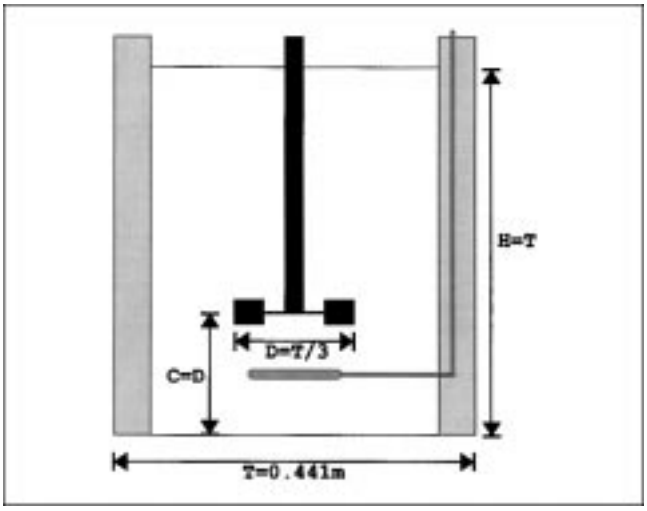

Figure 5. Geometry and dimensions of the baffled stirred vessel, equipped with a six-blade disc turbine and a ring sparger.

Numerical Procedure

Single-phase simulation

The starting point of the PBE calculations is a converged single-phase simulation which in our case is obtained with the commercial CFD-package FLUENT (version 4.40). In these simulations, the interaction of the rotating impeller with the surrounding liquid is modeled using a black-box approach, that is, experimentally determined velocities, kinetic energy, and viscous dissipation rates are presented at the impeller tip. Turbulence is modeled with the anisotropic Reynolds stress model. In Venneker and van den Akker (1997) and Venneker (1999) the single-phase predictions are compared with laser Doppler anemometry (LDA) measurements. Overall, the predictions are qualitatively correct, at least for the mean velocity field and with some room for improvement of the kinetic energy and energy dissipation. Also, due to the followed black-box approach, the predictions in the impeller region are not reliable.

Velocity field under gassed conditions

Before the gas dispersion model can be used, some considerations about the velocity field under gassed conditions must first be made. The presence of gas bubbles may affect the velocity field in several ways. In the wake of a bubble, some amount of liquid may be carried away along with the bubble. In regions with a positive (upward directed) axial velocity this effect may increase the axial velocity, while in regions with a downward directed flow, the absolute axial velocity is decreased. The velocity field under gassed conditions can be altered also by the gas cavities behind the impeller blades. The decrease in power input caused by these cavities decreases the pumping effect of the impeller and, thereby, the radial velocities in the discharge jet.

To obtain a reliable solution of the gas dispersion, the single-phase flow solution must therefore be corrected. The liquid flow field is altered here in a global way to account for the presence of gas bubbles. Based on the work of Roušar and van den Akker (1994), the power drop in gassed conditions is used to obtain the new flow field. The following correlations were used

$$U_g^* = U^* \cdot \left(\frac{P_g}{P}\right)^{0.65}$$

$$V_g^* = V^* \cdot \left(\frac{P_g}{P}\right)^{0.4}$$

$$W_g^* = W^* \cdot \left(\frac{P_g}{P}\right)^{0.65}$$

$$k_g^* = k^* \cdot \left(\frac{P_g}{P}\right)$$

$$\epsilon_g^* = \epsilon^* \cdot \left(\frac{P_g}{P}\right)^{2/3} \qquad (48)$$

where $*$ denotes dimensionless variables (with V_{tip}).

The scaling of the energy dissipation rate is slightly different. First, any discrepancy between single-phase simulation and the experiment is removed by assigning 18% of the power input to the impeller region (see the Large Eddy Simulations of Derksen and van den Akker (1998)). Next, the ϵ values in the bulk are corrected with the difference between single-phase simulation and experiment. Only then, the scaling to the gassed conditions is made according to Eq. 48.

Solving the PBEs

Given a converged 3-D single-phase flow solution, a 2-D field is obtained by averaging the results over the tangential direction. This is done to limit the computational time and memory. The calculated flow field is then corrected for any difference in power drawn between simulation and theory. Finally, the scaling to gassed conditions is made according to Eq. 48.

With the gas dispersion model, the startup of stirred vessel aeration is simulated. So the simulation starts with initially no gas in the tank, and as an inlet condition (at the sparger position) a prescribed gas-flow rate of bubbles with a fixed size. After all the PBEs have been solved at the new time step, the local and overall holdup values are calculated by summing up the volume occupied by each bubble class. A check is made whether the solution is converged or not, and whether somewhere the local holdup exceeds 100%. The solution is converged if the difference between the amount of gas leaving the vessel at the top and the amount of gas that enters the vessel is less than 0.1%.

Results of the PBE Model

In this section, results are presented for the simulation of the aerated Xanthan gum solution and compared where possible with measurements. The number of bubble classes in the simulation was taken as $M = 25$, with the smallest bubble size $d_1 = 0.125$ mm, and the largest $d_{25} = 32$ mm. The next sizes are twice as large in volume as the previous size. The

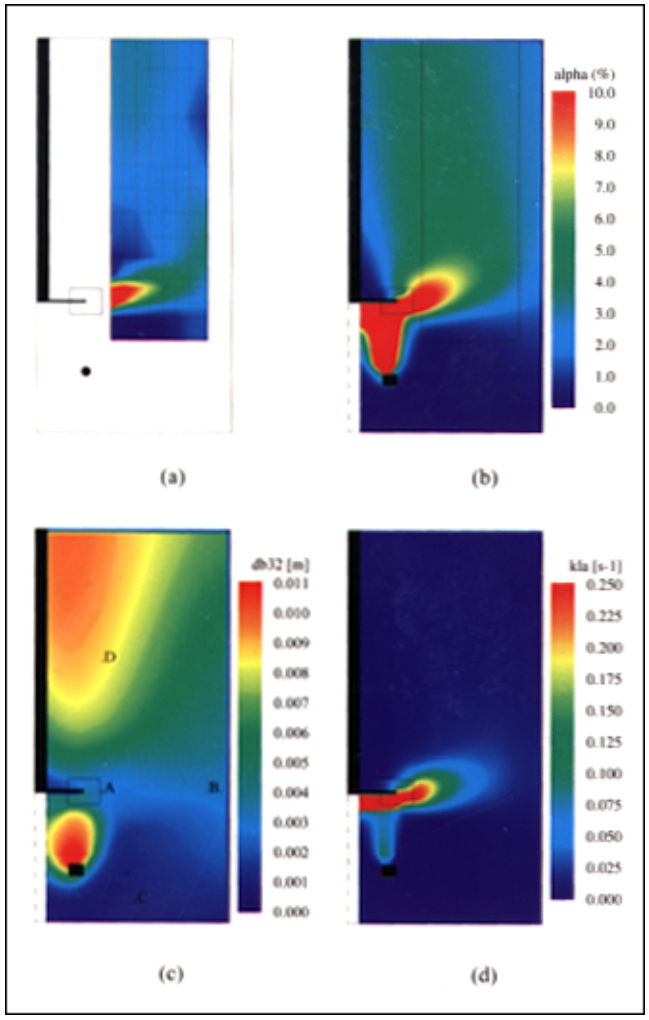

Figure 6. PBE simulation results of 0.075% Keltrol.

(a) Local gas fraction [%] in experiment; (b) predicted local gas fraction; (c) predicted Sauter mean diameter [m]; (d) predicted mass transfer coefficient [1/s]. Overall holdup experiment: $3.6\% \pm 0.2$; simulation: 3.08%. Overall $db_{32} = 5.19$ mm; Overall $k_l a = 0.0147$ 1/s.

limits were determined by examining the bubble-size distribution in each computational cell and making sure that the amount of bubbles in the first and last class are practically zero. Finally, a time step of 0.01 s was used.

In Figures 6a and 6b, contour plots of the experimentally and computationally determined local holdup values are shown. The measurements were performed at the intersection of the drawn lines. The red areas in the figure denote regions with gas fractions higher than 10%.

This figure clearly shows the potential strength of CFD in general and of DAWN in particular; the internal distribution of gas inside a stirred vessel can now be calculated and is with this first attempt using population balance equations quite comparable with experiments. The model is capable of predicting the essential features of this particular flow regime: high gas fractions above the sparger and in the impeller outflow; the concentration of gas in the upper part of the vessel; the accumulation of gas in the lower part of the vessel near the vessel wall; and the absence of gas beneath the sparger.

The reason why the two contour plots in Figure 6 are not identical can be contributed to more than one fact. First, the simulations are for an averaged 2-D field, whereas the measurements were performed in the plane between the baffles. Second, the errors in the gas fraction are to a large extent caused by errors in the calculated single-phase flow field and the subsequent scaling. With the solution strategy of DAWN, improvements in the (scaling of) single-phase flow field are easily extended to improvements in the gas fraction field. Also, in the formulation of DAWN, there is room for improvement. Eventually, a two-way coupling between the liquid and the gas is necessary. At present however, the theory on multiphase flow modeling is far from that point.

To perceive which future improvements are necessary, the simulation is now analyzed in more detail. The experiment shows a clear meandering of the gas fraction field in the upper part of the vessel. This meandering is caused by a small liquid recirculation loop near the wall in the top of the vessel. This effect can also be seen in the drawing of the bulk flow patterns in an aerated stirred vessel of Nienow et al. (1977). The meandering is absent in the simulation, which is not surprising because the secondary recirculation loop is also not present in the single-phase calculation. Clearly, a substantial change in flow direction due to the presence of gas cannot be predicted with this model.

A striking fact are the higher gas fractions (compared to experiments) in the bulk of the vessel. This can also be seen in Figure 7, where α-profiles are shown for different heights. The overall holdup in the simulation was, however, lower than obtained experimentally. The most plausible reason for this contradiction is the fact that not all bubbles were detected by the glass fiber probe. Bubbles smaller than 1 mm are not pierced at all by the probe, while larger bubbles are not detected when their approach direction is not in line with the probe tip.

Bubble Size and Mass-Transfer Predictions. As a final result, contour plots of the local Sauter mean bubble diameter db_{32} and the local mass-transfer coefficient $k_l a$ are presented (see Figures 6c and d). In Figure 6c, it can be seen that the smallest bubbles are localized in the lower part of the vessel, and not as one would expect, in the impeller region. This is caused for the following reason. Small bubbles are formed in the impeller region where turbulence intensity is highest. In that region, not all bubbles are broken; as a consequence, the minimum local value of db_{32} is not found in the impeller outflow. At the height where the impeller outflow reaches the vessel wall, the flow is divided into two circulation loops. The largest bubbly are mainly carried away with the upper loop, while small bubbles can be found in either loop. In the circulation loops, turbulence intensity is low. With increasing height, db_{32} increases because of coalescence. This occurs in both loops, which explains the relatively high bubble sizes in the lower corner of the vessel near the wall. From this latter region, only the smallest bubbles are taken away towards the impeller, while the larger bubbles have a sufficiently high slip velocity to escape and rise along the vessel wall. As a consequence, the region with the lowest db_{32} is found in the lower corner near the symmetry axis, which is a region with low gas fraction.

Bubble-size distributions in four characteristic positions in the vessel (see Figure 6c) are shown in Figure 8. Comparing

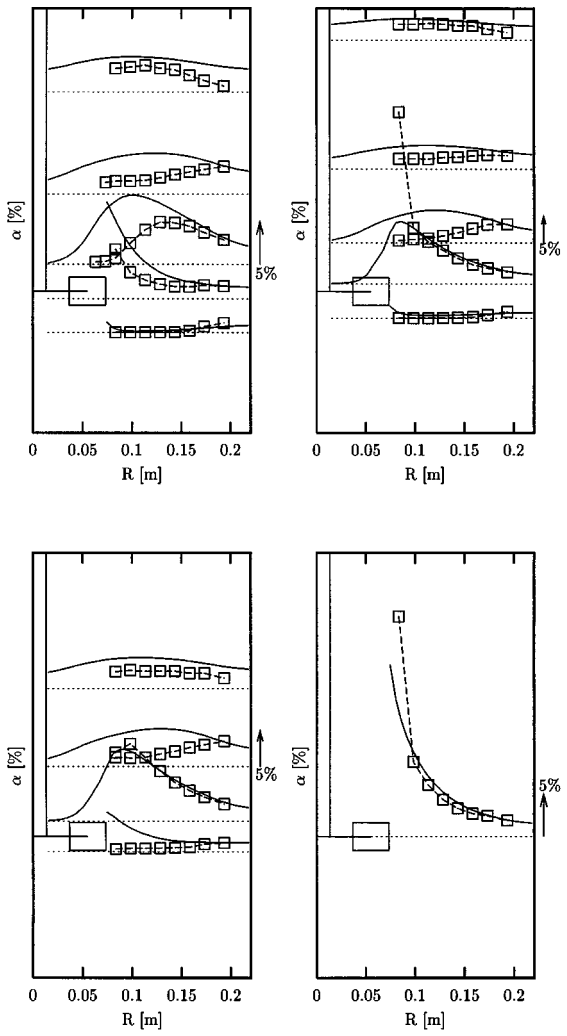

Figure 7. Measurements and predictions of the local gas fraction at several heights in 0.075% Keltrol.

Experimental conditions: $N = 5.0$ rev/s, $Q_g = 1.0$ L/s, $P_g = 0.275$ W/kg.

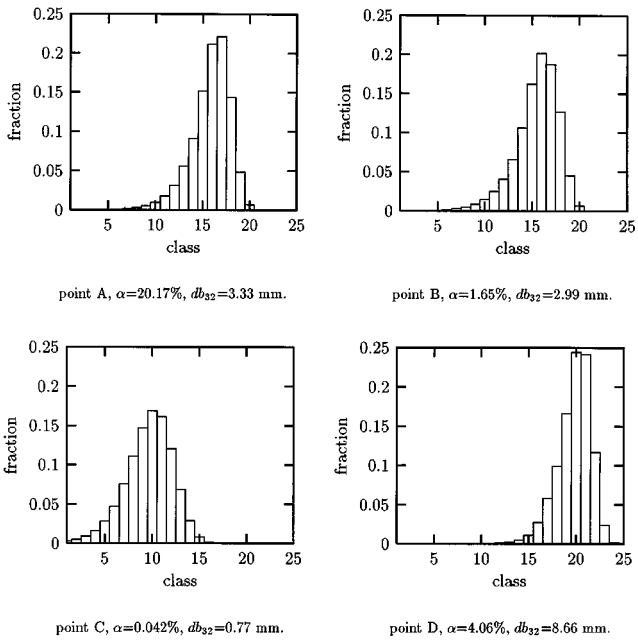

Figure 8. Bubble-size distribution as predicted by DAWN at characteristic positions in the vessel.

points A, close to the impeller tip, and B, close to the wall, we see at point B that more smaller bubbles are present and the class with the maximum number of bubbles has shifted from 17 to 16. The region with the highest fraction of smallest bubbles is found just above the vessel bottom, and point C shows a typical bubble-size distribution. Finally, point D shows the distribution in the quiescent region in the upper part of the tank where large bubbles are formed by coalescence.

The bubble-size histograms can serve as a third validation method, next to measurements of the overall and local values of the gas fraction, of the model. Experimentally determined bubble-size distributions can, for example, be obtained by a suction probe (Greaves and Barigou, 1988) or photographically (Takahashi and Nienow, 1993).

The ability of predicting local bubble-size distributions is the major advantage of the PBE formulation over two-fluid modeling. It offers the possibility of investigating the internal gas-liquid structure and can be used to improve the mass-transfer process.

The contour plot of $k_l a$ shows that mass transfer is far from uniform throughout the vessel, although the flow regime is completely dispersed. The highest values of $k_l a$ are found below the impeller disc and in the outflow of the impeller. It must be noted that in reality the bubble sizes directly beneath the impeller disc are not as small as predicted by the model. The specific area a is thus overpredicted there, meaning that the majority of the mass transfer occurs in the impeller outflow. Given this irregular distribution of $k_l a$, it is obvious why multiple impellers are used in practical situations.

Conclusions

A model has been presented based on the use of population balance equations to simulate the behavior of bubbles with different sizes in a turbulently agitated vessel. The interaction between liquid and gas was assumed to be 1.5 way coupled, and the liquid flow field is obtained from a single-phase flow simulation. With the model, local values of gas holdup, bubble size, number densities, and mass-transfer coefficients in an aerated stirred tank can be calculated. The model predictions concerning local gas holdup are comparable with experiments and are encouraging enough to conclude that the use of population balance equations is a promising technique to study dispersed flows. The main advantage of using PBEs is that bubble-bubble interactions are explicitly taken into account. Hence, research on mass transfer in dispersed flows can be carried out more accurately than with models with only one bubble size. In future work, the methodology as discussed in this article will be applied to

3-D, transient simulations of stirred tanks to realistically predict gas dispersion.

Acknowledgments

The authors thank Kim Vahl for improving the simulation procedure. This work was supported by the Netherlands Foundation for Chemical Research (SON) with financial aid from the Netherlands Technology Foundation (STW).

Notation

a = heigh of ellipse, m
a = radius of thinning disc, m
a = total specific bubble area, m^{-1}
a_b = surface area of bubble, m^2
A = Hamaker constant, $kg \cdot m^2 \cdot s^{-2}$
b = width of ellipse, m
B = birth function, $m^{-4} \cdot s^{-1}$
c = relative speed of a bubble, $m \cdot s^{-1}$
d = bubble diameter, m
db_{32} = Sauter mean bubble diameter, m
d_e = diameter of a volume-equivalent sphere, m
D = death function, $m^{-4} \cdot s^{-1}$
$\mathfrak{D}$ = diffusion coefficient, $m^2 \cdot s^{-1}$
e = energy of an eddy, $kg \cdot m^2 \cdot s^{-2}$
e = surface energy, $kg \cdot m^2 \cdot s^{-2}$
E = three-dimensional energy spectrum, $m^3 \cdot s^{-2}$
f_1, f_2 = fraction
g = breakage frequency, s^{-1}
h = effective swept volume rate, $m^3 \cdot s^{-1}$
h = film thickness, m
h_c = critical film thickness at rupture, m
h_0 = initial film thickness, m
k = kinetic energy of turbulence per unit of mass, $m^2 \cdot s^{-2}$
k = wave number, m^{-1}
k_l = mass-transfer coefficient, $m \cdot s^{-1}$
K = consistency, $kg \cdot s^{n-2} \cdot m^{-1}$
l_d = Kolmogorov length micro scale, m
m_λ = mass of an eddy, kg
M = number of bubble classes
n = number density probability, m^{-4}
n_λ = number density probability of eddies, m^{-4}
n = flow index
N = impeller rotational speed, s^{-1}
N = number density, m^{-3}
p = coalescence efficiency
p_b = breakage efficiency
P = power draw impeller, $W \cdot kg^{-1}$
Q_g = gas-flow rate, $m^3 \cdot s^{-1}$
r = bubble radius, m
r = radial co-ordinate, m
R_{eq} = equivalent bubble radius, m
t = time, s
$\tilde{t}$ = drainage time, s
t_e = exposure time, s
t_{mob} = drainage time for deformable fully mobile interfaces, s
T = tank diameter, m
T^+ = dimensionless bursting time
u = bubble velocity, $m \cdot s^{-1}$
u_c = critical eddy velocity, $m \cdot s^{-1}$
u_g = gas velocity, $m \cdot s^{-1}$
u_k = eddy velocity as function of wave number, $m \cdot s^{-1}$
$u_{l,g}$ = liquid velocity under gassed conditions, $m \cdot s^{-1}$
u_s = bubble slip velocity, $m \cdot s^{-1}$
u_λ = eddy velocity as function of eddy size, $m \cdot s^{-1}$
U = mean axial velocity, $m \cdot s^{-1}$
v = characteristic velocity, $m \cdot s^{-1}$
V = approach velocity between bubbles, $m \cdot s^{-1}$
V = mean radial velocity, $m \cdot s^{-1}$
W = mean tangential velocity, $m \cdot s^{-1}$
x = bubble diameter, m
z = height co-ordinate, m

Greek letters

α = gas fraction
ϵ = dissipation rate of turbulent kinetic energy, $m^2 \cdot s^{-3}$
η = daughter probability distribution, m^{-1}
λ = eddy size ($= k/2\pi$), m
ν = number of bubbles formed by breakage
ν_0 = friction velocity, $m \cdot s^{-1}$
ρ_c = density of continuous phase, $kg \cdot m^{-3}$
σ = surface tension, $kg \cdot s^{-2}$
τ = eddy turnover time, s
ω = eddy-bubble collision rate, $m^{-1} s^{-1}$

Subscripts

b = bubble related variable
g = gassed condition
i, j, j = class index
λ = eddy related variable

Dimensionless groups

C_d = drag coefficient, $4\Delta\rho g d/3\rho u_s^2$
Eo = Eötvös number, $g\rho_c d_e^2/\sigma$
Re_b = bubble Reynolds number, $\rho_c u_s^{2-n} d^n/K$
Sc = Schmidt number, $\nu/\mathfrak{D}$
We = Weber number, $\rho_c u^2 d/\sigma$

Literature Cited

Bakker, A., "Hydrodynamics of Stirred Gas-Liquid Dispersions," PhD Thesis, Delft Univ. of Technology (1992).
Bakker, A., and H. E. A. van den Akker, "A Computational Model for the Gas-Liquid Flow in Stirred Reactors," *Trans. Inst. Chem. Eng.*, **72**, 594 (1994).
Barnett, S. M., A. E. Humphrey, and M. Litt, "Bubble Motion and Mass Transfer in Non-Newtonian Fluids," *AIChE J.*, **12**, 253 (1966).
Batchelor, G. K., "Pressure Fluctuations in Isotropic Turbulence," *Proc. Camb. Phil. Soc.*, **47**, 359 (1951).
Chesters, A. K., "The Applicability of Dynamic-Similarity Criteria to Isothermal, Liquid-Gas, Two-Phase Flows without Mass Transfer," *Int. J. Multiphase Flow*, **2**, 191 (1975).
Chesters, A. K., "The Modelling of Coalescence Processes in Fluid-Liquid Dispersions: A Review of Current Understanding," *Trans. Inst. Chem. Eng.*, **69**, 25 (1991).
Clift, R., J. R. Grace, and M. E. Weber, *Bubbles, Drops and Particles*, Academic Press (1978).
Coulaloglou, C. A., and L. L. Tavlarides, "Description of Interaction Processes in Agitated Liquid-Liquid Dispersions," *Chem. Eng. Sci.*, **32**, 1289 (1977).
Danckwerts, P. V., "Significance of Liquid-Film Coefficients in Gas Absorption," *Ind. Eng. Chem.*, **43**, 1460 (1951).
Derksen, J. J., and H. E. A. van den Akker, "Parallel Simulation of Turbulent Fluid Flow in a Mixing Tank," Lecture Notes in Computer Science—High-performance Computing and Networking, P. Sloot, M. Bubak, and B. Hertzberger, eds., Vol. 1401, p. 96 (1998).
Djebbar, R., M. Roustan, and A. Line, "Numerical Computation of Turbulent Gas-Liquid Dispersions in Mechanically Agitated Vessels," *Trans. Inst. Chem. Eng.*, **74**, 492 (1996).
Gosman, A. D., C. Lekakou, S. Politis, R. I. Issa, and M. K. Looney, "Multidimensional Modelling of Turbulent Two-Phase Flows in Stirred Vessels," *AIChE J.*, **38**, 1946 (1992).
Grace, J. R., T. Wairegi, and T. H. Nguyen, "Shapes and Velocities of Single Drops and Bubbles Moving Freely Through Immiscible liquids," *Trans. Inst. Chem. Eng.*, **54**, 167 (1976).
Greaves, M., and M. Barigou, "The Internal Structure of Gas-Liquid Dispersions in a Stirred Reactor," *Eur. Conf. on Mixing*, Pavia, Italy, p. 313 (May 24–26, 1988).

Haque, M. W., K. D. P. Nigam, K. Viswanathan, and J. B. Joshi, "Studies on Bubble Rise Velocity in Bubble Columns Employing Non-Newtonian Solutions," *Chem. Eng. Commun.*, **73**, 31 (1988).
Harmathy, T. Z., "Velocity of Large Drops and Bubbles in Media of Infinite or Restricted Extent," *AIChE J.*, **6**, 281 (1960).
Hesketh, R. P., A. W. Etchells, and T. W. F. Russell, "Experimental Observations of Bubble Breakage in Turbulent Flow," *Ind. Eng. Chem. Res.*, **30**, 835 (1991).
Higbie, R., "The Rate of Absorption of a Pure Gas into a Still Liquid During Short Periods of Exposure," *Trans. AIChE*, **31**, 365 (1935).
Hinze, J. O., *Turbulence (second edition)*, McGraw-Hill, New York (1975).
Hulburt, H. M., and S. L. Katz, "Some Problems in Particle Technology. A Statistical Mechanical Formulation," *Chem. Eng. Sci.*, **19**, 555 (1964).
Ishii, M., *Thermo-fluid Dynamic Theory of Two-Phase Flow*, Eyrolles (1975).
Issa, R. I., and A. D. Gosman, "The Computation of Three-Dimensional Turbulent Two-Phase Flows in Mixer Vessels," *2nd Int. Conf. Numerical Methods in Laminar and Turbulent Flow*, p. 827 (1981).
Jenne, M., and M. Reuss, "Fluid Dynamic Modelling and Simulation of Gas-Liquid Flow in Baffled Stirred Tank Reactors," *Mixing IX. Recent Advances in Mixing*, J. Bertrand and J. Villermaux, eds., 201 (1997).
Kawase, Y., B. Halard, and M. Moo-Young, "Theoretical Prediction of Volumetric Mass Transfer Coefficients in Bubble Columns for Newtonian and Non-Newtonian Fluids," *Chem. Eng. Sci.*, **42**, 1609 (1987).
Kawase, Y., and J. J. Ulbrecht, "Turbulent Heat and Mass Transfer in Non-Newtonian Pipe-Flow: a Model Based on the Surface Renewal Concept," *Phys. Chem. Hydr.*, **4**, 351 (1983).
Kirkpatrick, R. D., and M. J. Lockett, "The Influence of Approach Velocity on Bubble Coalescence," *Chem. Eng. Sci.*, **29**, 2363 (1974).
Kolmogorov, A. N., "Local Structure of Turbulence in Incompressible Viscous Fluid for Very Large Reynolds Number," *Dokl. Akad. Nauk SSSR*, **30**, 229 (1941).
Kuboi, R., I. Komasawa, and T. Otake, "Behavior of Dispersed Particles in Turbulent Liquid Flow," *J. Chem. Eng. Jap.*, **5**, 349 (1972).
Lathouwers, D., and H. E. A. van den Akker, "A Numerical Method for the Solution of Two-Fluid Model Equations," *Numerical Methods for Multiphase Flow, FED*, Vol. 236, p. 121 (1996).
Levich, V. G., *Physicochemical Hydrodynamics*, Prentice-Hall, Englewood Cliffs, NJ (1962).
Lewalle, J., L. L. Tavlarides, and V. Jairazbhoy, "Modeling of Turbulent, Neutrally Buoyant Droplet Suspensions in Liquids," *Chem. Eng. Comm.*, **59**, 15 (1987).
Luo, H., and H. F. Svendsen, "Theoretical Model for Drop and Bubble Breakup in Turbulent Dispersions," *AIChE J.*, **42**, 1225 (1996).
Mendelson, H. D., "The Prediction of Bubble Terminal Velocities from Wave Theory," *AIChE J.*, **13**, 250 (1967).
Metkin, V. P., and V. N. Sokolov, "Hydraulic Resistance to Flow of Gas-Liquid Mixtures Having Non-Newtonian Properties," *J. Appl. Chem. USSR*, **55**, 558 (1982).
Morud, K. E., and B. H. Hjertager, "LDA Measurements and CFD Modelling of Gas-Liquid Flow in a Stirred Vessel," *Chem. Eng. Sci.*, **51**, 233 (1996).
Nienow, A. W., D. J. Wisdom, and J. C. Middleton, "The Effect of Scale and Geometry on Flooding, Recirculation, and Power in Gassed Stirred Vessels," *2nd Eur. Conf. on Mixing*, Cambridge, U.K., 1 (1977).
Pinczewski, W. V., and S. Sideman, "A Model for Mass (Heat) Transfer in Turbulent Tube Flow. Moderate and High Schmidt (Prandtl) Numbers," *Chem. Eng. Sci.*, **29**, 1969 (1974).
Prince, M. J., and H. W. Blanch, "Bubble Coalescence and Break-Up in Air-Sparged Bubble Columns," *AIChE J.*, **36**, 1485 (1990).
Ramkrishna, D., "The Status of Population Balances," *Rev. in Chem. Eng.*, **3**, 49 (1985).
Richardson, J. F., and W. F. Zaki, "Sedimentation and Fluidisation: I," *Trans. Inst. Chem. Engrs.*, **32**, 35 (1954).
Ritchie, B. W., and A. H. Togby, "General Population Balance Modelling of Unpremixed Feedstream Chemical Reactors: a Review," *Chem. Eng. Comm.*, **2**, 249 (1978).
Roušar, I., and H. E. A. van den Akker, "LDA Measurements of Liquid Velocities in Sparged Agitated Tanks with Single and Multiple Rushton Turbines," *8th Eur. Conf. on Mixing*, Cambridge, U.K., 89 (Sept. 21–23, 1994).
Takahashi, K., and A. W. Nienow, "Bubble Sizes and Coalescence Rates in an Aerated Vessel Agitated by a Rushton Turbine," *J. Chem. Eng. Jap.*, **26**, 536 (1993).
Tennekes, H., and J. L. Lumley, *A First Course in Turbulence*, MIT Press, Cambridge, MA (1972).
Tsouris, C., and L. L. Tavlarides, "Breakage and Coalescence Models for Drops in Turbulent Dispersions," *AIChE J.*, **40**, 395 (1994).
Tsukada, T., H. Mikami, M. Hozawa, and N. Imaishi, "Theoretical and Experimental Studies of the Deformation of Bubbles Moving in Quiescent Newtonian and Non-Newtonian Liquids," *J. Chem. Eng. Jap.*, **23**, 192 (1990).
van Santen, H., D. Lathouwers, C. R. Kleijn, and H. E. A. van den Akker, "Influence of Segregation on the Efficiency of Finite Volume Methods for the Incompressible Navier-Stokes Equations," *Proc. of Fluid Eng. Div. of ASME*, Vol. 3, FED Vol. 238, 151 (1996).
Venneker, B. C. H., "Turbulence Flow and Gas Dispersion in Stirred Vessels with Pseudo-Plastic Liquids," PhD Thesis, Delft University of Technology (1999).
Venneker, B. C. H., and H. E. A. van den Akker, "CFD Calculations of the Turbulent Flow of Shear-Thinning Fluids in Agitated Tanks," *Mixing IX. Recent Advances in Mixing*, J. Bertrand and J. Villermaux, eds., 179 (1997).
Wallis, G. B., "The Terminal Speed of Single Drops or Bubbles in an Infinite Medium," *Int. J. Multiphase Flow*, **1**, 491 (1974).

Manuscript received Mar. 29, 2001, and revision received Oct. 1, 2001.